

Probe-based bacterial single-cell RNA sequencing predicts toxin regulation

Received: 9 January 2023

Accepted: 25 February 2023

Published online: 03 April 2023

 Check for updates


Ryan McNulty^{1,2,9}, Duluxan Sritharan^{3,4,9}, Seong Ho Pahng^{5,4}, Jeffrey P. Meisch¹, Shichen Liu⁴, Melanie A. Brennan¹, Gerda Saxer¹, Sahand Hormoz^{6,7}  
& Adam Z. Rosenthal^{1,8}  

Clonal bacterial populations rely on transcriptional variation across individual cells to produce specialized states that increase fitness. Understanding all cell states requires studying isogenic bacterial populations at the single-cell level. Here we developed probe-based bacterial sequencing (ProBac-seq), a method that uses libraries of DNA probes and an existing commercial microfluidic platform to conduct bacterial single-cell RNA sequencing. We sequenced the transcriptome of thousands of individual bacterial cells per experiment, detecting several hundred transcripts per cell on average. Applied to *Bacillus subtilis* and *Escherichia coli*, ProBac-seq correctly identifies known cell states and uncovers previously unreported transcriptional heterogeneity. In the context of bacterial pathogenesis, application of the approach to *Clostridium perfringens* reveals heterogeneous expression of toxin by a subpopulation that can be controlled by acetate, a short-chain fatty acid highly prevalent in the gut. Overall, ProBac-seq can be used to uncover heterogeneity in isogenic microbial populations and identify perturbations that affect pathogenicity.

Bacterial traits such as competence, sporulation and motility have been shown to be both heterogeneously utilized in populations and tightly controlled at the transcriptional level, emphasizing the need for single-cell transcriptional analyses^{1–3}. However, tools for single-cell RNA sequencing (scRNA-seq) of bacterial populations remain limited due to several substantial technical challenges. First, total bacterial messenger RNA (mRNA) abundance is two orders of magnitude lower than that of eukaryotes, with a single bacterial cell containing approximately 10^3 – 10^4 transcripts during exponential growth⁴. Second, transcriptional turnover is much faster in bacteria, with an mRNA half-life on the scale of minutes, compared with hours in eukaryotes⁴. Third, bacterial transcripts do not intrinsically include a 3' poly-adenosine tail

and, therefore, mRNA cannot easily be tagged and selectively enriched against ribosomal RNA, which makes up more than 90% of the bacterial transcriptome⁴. Lastly, accessing mRNA requires cell permeabilization, which is difficult in bacteria due to the diversity in membrane structures and variability of the peptidoglycan layer.

We reasoned that a method combining the advantages of microfluidic single-cell barcoding in droplets with the ability to tag transcripts using in situ hybridization of oligonucleotide probes could overcome these challenges and offer advantages over alternative approaches^{5–7}. Here we present a method called probe-based bacterial sequencing (ProBac-seq) for prokaryotic scRNA-seq, which uses a commercial, benchtop microfluidic device (Chromium Controller

¹IFF Health and Biosciences, Wilmington, DE, USA. ²Lewis-Sigler Institute for Integrative Genomics, Princeton University, Princeton, NJ, USA. ³Harvard Graduate Program in Biophysics, Harvard University, Cambridge, MA, USA. ⁴Department of Data Science, Dana-Farber Cancer Institute, Boston, MA, USA. ⁵Department of Chemistry and Chemical Biology, Harvard University, Cambridge, MA, USA. ⁶Department of Systems Biology, Harvard Medical School, Boston, MA, USA. ⁷Broad Institute of MIT and Harvard, Cambridge, MA, USA. ⁸Department of Microbiology and Immunology, University of North Carolina, Chapel Hill, NC, USA. ⁹These authors contributed equally: Ryan McNulty, Duluxan Sritharan.  e-mail: Sahand_Hormoz@hms.harvard.edu; Adam_Rosenthal@med.unc.edu

from 10X Genomics) and custom single-stranded DNA probe libraries to resolve the mRNA profile of thousands of bacterial cells.

Results

Probe design and library generation

To leverage existing microfluidic single-cell sequencing platforms, we devised a method whereby individual transcripts are tagged with DNA probes. This approach requires generating large oligonucleotide libraries that are complementary to the protein-coding sequences within a genome (Supplementary Fig. 1). Large transcriptome-wide oligonucleotide libraries have been extensively used for bulk transcriptomics in microarrays and, more recently, to selectively capture mRNA from an infection model that includes mammalian and bacterial transcripts⁸. In our design, multiple DNA regions of 50 base pairs (bp) were chosen from each open-reading frame based on uniqueness as determined by UPS2 software⁹ or based on published oligonucleotide arrays^{10,11}. These sequences then served as the target regions of single-stranded DNA probes, which were designed to hybridize to the corresponding mRNA by sequence complementarity. Probes also contained a 5' polymerase chain reaction (PCR) handle for library generation, a unique molecular identifier (UMI) and a 3' poly-A tail (A₃₀) for retrofitting prokaryotic transcripts to the 10X Genomics Single Cell 3' system (Fig. 1a). Multiple probes (complementary to different regions) were designed for each gene to enhance transcript-capture efficiency and decrease noise caused by poor hybridization and/or insufficient amplification of any given probe. Complete species libraries contained 29,765 probes for *Bacillus subtilis*, 21,527 probes for *Escherichia coli* and 11,723 probes for *Clostridium perfringens* and targeted 2,959 (*B. subtilis*) 4,181 (*E. coli*) and 3,189 (*C. perfringens*) genes, respectively. Libraries were ordered at subfemtomole quantities from Twist Biosciences (a one-time cost of US\$0.05–0.15 per probe) and amplified by rolling circle amplification¹² to obtain a sufficient amount (0.25 mg = 10.25 nmol per library or approximately 0.35 pmol of each probe) for scRNA-seq experiments (Methods, Supplementary Tables 1–3 and Supplementary Figs. 1 and 2). Probe libraries were completed by addition of randomized 12 bp UMI sequences and a poly-A tail and purified. Read coverage across completed probe libraries was well approximated by a log normal distribution (Supplementary Fig. 1e). The rolling circle amplification approach permits re-amplifying probe sets for unlimited subsequent experiments without the need to re-order probes, at an upfront cost of under US\$0.01 per cell (Supplementary Table 4).

Before microfluidic encapsulation, bacteria were fixed in 1% paraformaldehyde to preserve transcripts and permeabilized by mild lysozyme treatment. Permeabilized bacteria were then incubated with the corresponding DNA probe library. Non-hybridized probes were removed with repeated washes (Fig. 1, Methods). Next, bacteria were run through a 10X Chromium Controller, where DNA probes were captured and barcoded in a manner analogous to the barcoding of the transcriptome of eukaryotic cells (Fig. 1b–d). The resulting libraries were sequenced, preprocessed with custom scripts extracting the target sequence, cell barcode and UMI (https://gitlab.com/hormozlab/bacteria_scrnaseq) and analysed with the standard CellRanger pipeline and the Seurat analysis package (Methods)^{13,14}.

Fig. 1 | Microfluidic probe-based scRNA-seq method and validation. **a**, Cells were fixed and permeabilized to allow the penetration of thousands of unique, genome-specific oligonucleotide probes. Hybridized probes retrofitted transcripts with a poly-A tail and UMI, whereas unhybridized probes were washed away. **b**, Permeabilized cells with hybridized probes were flowed through a commercial microfluidic device that encapsulates single cells into droplets containing barcoded primers with poly-A capture sequence conjugated to a hydrogel microsphere and PCR reagents. **c**, Final droplets contain one or fewer cells and one hydrogel with a unique cell barcode. Barcoded cDNA was generated from the mRNA:probe hybridized complex via in-droplet PCR. Droplets were then broken and the pooled cDNA amplified further before

Bacterial scRNA-seq validation

To determine if suspended probe libraries can report on the transcriptional state of cells, we split a culture of *B. subtilis* cells in a late exponential state into two aliquots of approximately 10⁸ formaldehyde-fixed cells each. One aliquot was processed using a traditional RNA-seq protocol (Methods), whereas the second sample was processed by in situ hybridization with the *B. subtilis* probe set. After hybridization and washing, the probes that remained bound were amplified by PCR and processed into Illumina libraries. The output from each method was compared. A probe-based library prepared with hybridization and wash conditions at 50 °C gave results similar to traditional RNA-seq (Fig. 1e; Pearson's $r = 0.73$). Repeating in *E. coli* with its respective probe set, we observed a Pearson correlation of 0.77 (Supplementary Fig. 19). These values are comparable to the correlation between RNA-seq and microarray experiments ($r = 0.75–0.80$)^{15,16}.

Next, we tested if single-cell transcriptomes can be captured by encapsulating individual bacteria using the 10X Chromium Controller. *E. coli* and *B. subtilis* cells were independently fixed and pretreated with probes corresponding to their respective genomes. The prepared bacterial samples were subsequently mixed and loaded onto a microfluidic chip along with a PCR master mix containing a DNA primer designed to amplify the back-end PCR handle built into the probes (Supplementary Fig. 1, Methods). This custom mix replaced the standard cDNA reagents supplied by 10X Genomics as the aqueous phase within the droplets. Sequenced libraries from this experiment demonstrate that the microfluidic platform can successfully segregate and barcode individual microbial cells (Fig. 1f). We observed a corrected multiplet rate of 2.8% for 3,373 captured cells, consistent with the expected rate of successful single-cell encapsulation based on the specifications of the 10X microfluidic system (expected 2.4% multiplet events per 3,000 recovered cells).

To assess whether the signal from individually encapsulated cells provides a representative readout of the transcriptomic state of the population, we compared the output produced by capturing probes from a bulk sample of cells ($\approx 10^8$ cells) to the signal obtained by summing the probe counts over thousands of individually tagged cells (aggregated UMIs). The abundances across probes between the two samples were highly correlated ($r = 0.94$, Fig. 1g), confirming the signal from single cells provides a good representation of transcriptional states.

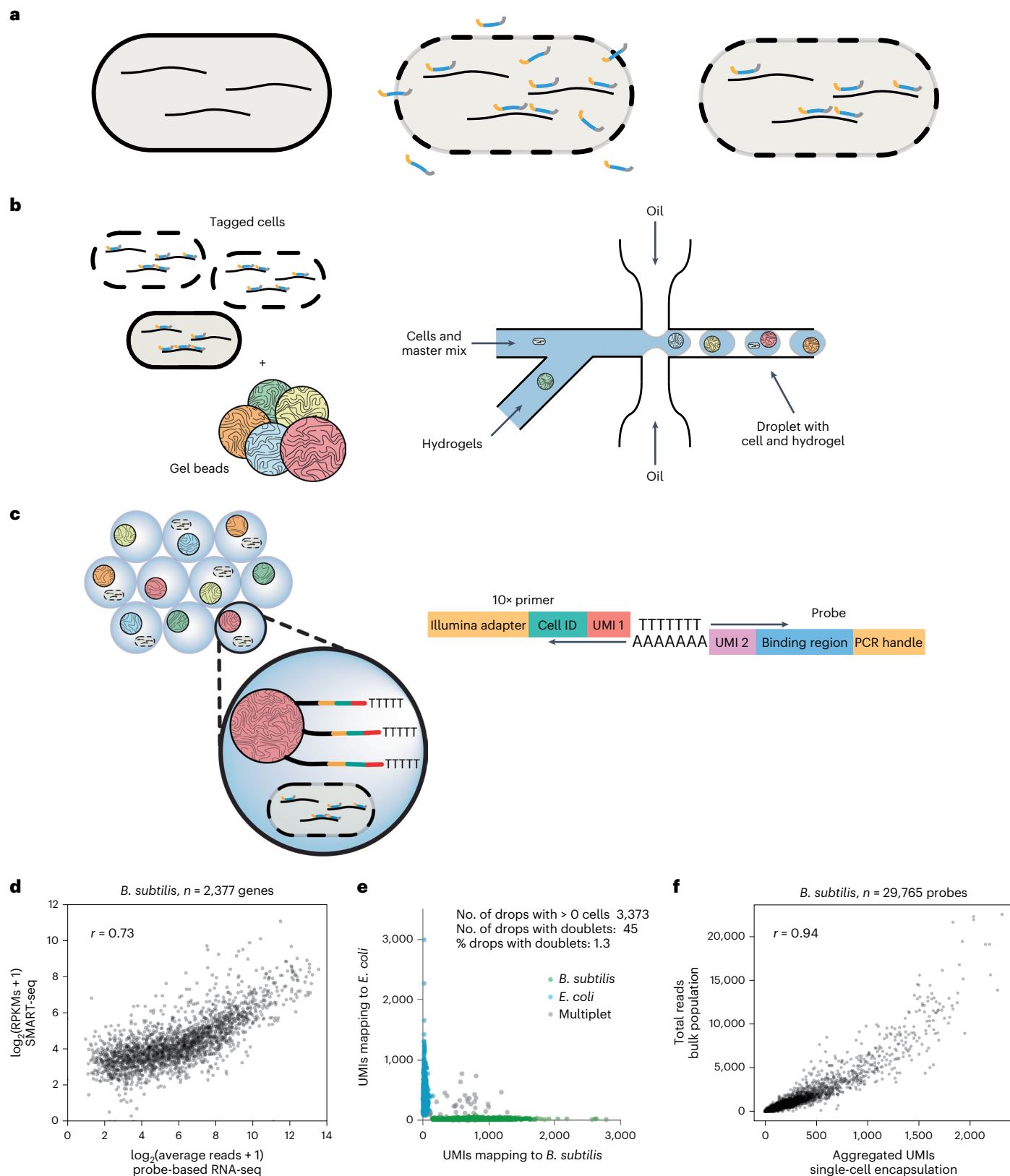
ProBac-seq identifies heterogeneity in *B. subtilis*

We performed ProBac-seq on *B. subtilis* grown to late exponential phase in M9 minimal media supplemented with malate. In total, 2,784 cells were captured as determined by unique barcodes at an average depth of 1,073 reads per cell. We detected a median of 325 mRNA transcripts per cell (approximately 10–20% of the total mRNA pool^{4,17}) corresponding to a median of 241 genes per cell. UMIs per probe ranged from 0 to 45 for any given gene in any given cell. The most highly detected probes targeted genes encoding ribosomal proteins (*rpsG*, *rpsH*, *rpsR*, *rpsM*, *rpsS*, *rplL*, *rplD*, *rplO*, *rplV*), translation elongation machinery (*fusA*, *tufA*, *map*) and transcriptional machinery (*rpoA*).

sequencing. Single-cell transcriptomes were resolved, clustered and visualized. **d**, Transcriptome quantification by hybridization of a probe library followed by PCR correlates (Pearson's correlation coefficient, $r = 0.73$) to traditional, bulk RNA-seq method (SMART-seq stranded kit, Takara) involving random priming of hexamers followed by reverse transcription (RT) and incorporation of template switching oligo. **e**, Species mixture ('barnyard') plot demonstrates that single cells of different bacterial species can be resolved by barcode after microfluidic encapsulation. **f**, Aggregated probe-based signal from thousands of single cells is well correlated (Pearson's correlation coefficient, $r = 0.94$) to the average probe-based signal obtained from the bulk population (pre-encapsulation). RPKM, reads per kilobase of exon per million reads mapped.

Next, we resolved distinct cellular states by dimensional reduction of single-cell expression vectors followed by graph-based clustering and analysis of differential gene expression (DGE) using the Seurat package and two-sided Wilcoxon rank-sum test with Bonferroni correction¹³. For *B. subtilis* in M9 minimal media in late log growth, we resolved four major transcriptomic states comprising

10 cell clusters that capture subtler signatures in gene expression (Fig. 2a,b, Supplementary Fig. 3 and Supplementary Table 6). Algorithmic grouping of cell-expression profiles was robust to the clustering parameters (Methods). As expected for *B. subtilis* at late log phase in minimal media, we observed a subpopulation of cells (clusters 6 and 8) with signatures of genetic competence. Cells in these two clusters



differentially overexpress the competence master-regulator, *comK*, compared with the rest of the population (\log_2 fold change (FC) = 2.37, adjusted P value = 4×10^{-179}) and multiple genes within and downstream of competence operons (*comC*, *G*, *E* and *F* operons, *coiA*, *dprA*, *sbB*, *nuca*, *nin*, *clpC* and *recA*). The fraction of competent cells in the population was measured by the fluorescence microscopy using a fluorescent promoter-reporter of *comGE* (Methods, Fig. 2c left panel and Supplementary Fig. 4a) and determined to be approximately 10.4% (interquartile range (IQR) outlier detection; Methods) similar to the fraction of the population comprising clusters 6 and 8 (9.3%, Supplementary Table 5). In total, we found that 45 of the 50 *comK* regulon genes that were targeted with probes were differentially overexpressed in clusters 6 and 8 (adjusted P values < 0.05; Fig. 2d and Supplementary Table 6). Our results agree with numerous studies identifying the competence regulon in *B. subtilis*^{18,19} and the percentage of cells displaying natural competence falls within previous observations for similar media (3–10%)^{20,21}.

Unexpectedly, for these growth conditions we observed a small subpopulation of cells within the sample (cluster 9, 19 cells, 0.7% of the population) with a transcriptomic signature indicative of sporulation. In these cells, we observed significant upregulation of transcripts corresponding to sigma factors associated with sporulation, *sigF* (\log_2 FC = 1.2, adjusted P value = 4×10^{-41}) and *sigG* (\log_2 FC = 2.2, adjusted P value = 2×10^{-63}), and genes in the *ger*, *cot* and *spoIVF* operons. Gene set enrichment analysis (GSEA) on all significantly upregulated genes in cluster 9 using ontological classes from the Gene Ontology Consortium^{22–24} reveals a 4.3-fold enrichment of genes involved in sporulation (false discovery rate (FDR) = 1×10^{-16} , Fisher's exact test) and spore germination (fold enrichment = 8.1, FDR = 1.7×10^{-3}). This finding highlights ProBac-seq's ability to detect rare and unexpected cell states. To confirm this subpopulation, we created a promoter-reporter for *cotY*, a spore coat gene expressed in the sporulating mother cell. Fluorescence observation identifies the presence of *cotY* expression and spores in a similar percentage of cells as recovered by scRNA-seq (0.5–1%) (Fig. 2c middle panel, Supplementary Fig. 4d).

The largest grouping of *B. subtilis* cells (comprising clusters 1, 2, 3, 5 and part of 7) accounted for ~45% of the population and was characterized primarily by the upregulation of the *dhb* operon (\log_2 FCs > 0.25, adjusted P values < 2×10^{-5}). Genes *dhbA*, *dhbB*, *dhbC*, *dhbE* and *dhbF* encode the five enzymes implicated in the biosynthesis of bacillibactin—a catecholic siderophore that is produced and secreted in response to intracellular iron deprivation. Relatedly, *yusV*, which encodes an ABC transporter of bacillibactin, was also upregulated in these cells. Cells within cluster 5 are distinguished from the rest of the subpopulation by expression of genes related to arginine biosynthesis via ornithine. In total, 10 of 14 genes associated with the cellular process were significantly upregulated in this cluster alone (gene set fold enrichment = 19.35, FDR = 3×10^{-8}). A fluorescent promoter-reporter for *argC* confirms heterogeneous expression of arginine genes with approximately 2.1% of cells in the high-*argC* expressing tail of the distribution, compared with 7.2% of cells in this state as determined by scRNA-seq (Fig. 2c right panel, Methods, Supplementary Fig. 4b and Supplementary Table 5).

Prokaryotes often express genes with related functions as operons; polycistronic transcripts under the control of a single promoter. In many cases, we observed genes of the same operon overexpressed within the same cluster of cells, serving as an internal control for our RNA capture and clustering methods. To further explore the ability of ProBac-seq to resolve operons agnostically, pairwise comparisons of gene expression levels across cells were computed using Spearman distance as a measure of covariance. Pairwise distances were then related by agglomerative hierarchical clustering (average linkage) to identify sets of covarying genes. Compared to scrambled controls, genes with significant covariance (empirical P value < 3×10^{-5}) often recapitulated known operons in *B. subtilis* (Supplementary Fig. 5 and Supplementary Table 7), providing strong evidence that probes capture true transcriptomic signatures across individual cells.

Taken together, our platform for single-cell sequencing of individual bacterium correctly recapitulates the known cellular states of *B. subtilis* at the expected population fractions and identifies previously unreported cellular states and was able to uncover features of the underlying genomic architecture.

Expression heterogeneity in a clonal *E. coli* population

With a validated method for identifying cellular states in *B. subtilis*, we used ProBac-seq to characterize transcriptional heterogeneity in *E. coli* MG1655 that was grown in M9 minimal media and chemically fixed at an optical density $OD_{600} = 0.5$ (mid-log phase). We resolved 3,315 cells at an average depth of 1,070 reads per cell, detecting a median of 263 transcripts per cell representing a median of 165 distinct genes. Cells were partitioned into nine groups by graph-based clustering of their gene expression profiles (Fig. 3a,b, Supplementary Fig. 6 and Supplementary Table 6). As with *B. subtilis*, we observe that certain clusters can be assigned to specific biological processes by DGE and that cluster determination is robust to the choice of clustering parameters (Methods). For example, cells in cluster 1 (482 cells, 14.5% of population) uniquely upregulate genes implicated in cell motility, including those encoding chemotaxis signalling proteins (*cheA*, *cheW*, *tar*; gene set fold enrichment > 100, FDR = 3.1×10^{-2}) and structural flagella components (*flhC*, *flgL*, *flgG*, *flgD*, *flgE*, *flgC*, *flgF*; gene set enrichment = 86.08, FDR = 2.6×10^{-6}). This list includes genes regulated by class 1, 2 and 3 flagella promoters; three distinct regulons that control the sequential expression of flagella genes including the master-regulator *flhDC*, components of the membrane-associated basal body and chemotaxis proteins, respectively²⁵. To confirm the presence of a motile subpopulation of cells, we stained cells grown under the same conditions using Remel Flagella Stain and visualized them through phase microscopy (Fig. 3d). This revealed that approximately 36% of cells had assembled flagella, which was a greater proportion than the 14.5% observed in the scRNA-seq cluster 1. A possible explanation for this discrepancy is that some flagellated cells may have already exited the transcriptional state, but still retained the translated protein product.

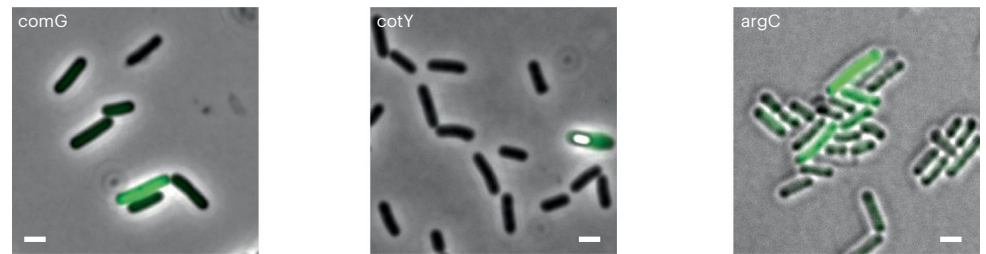
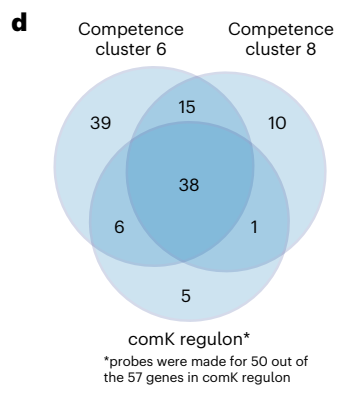
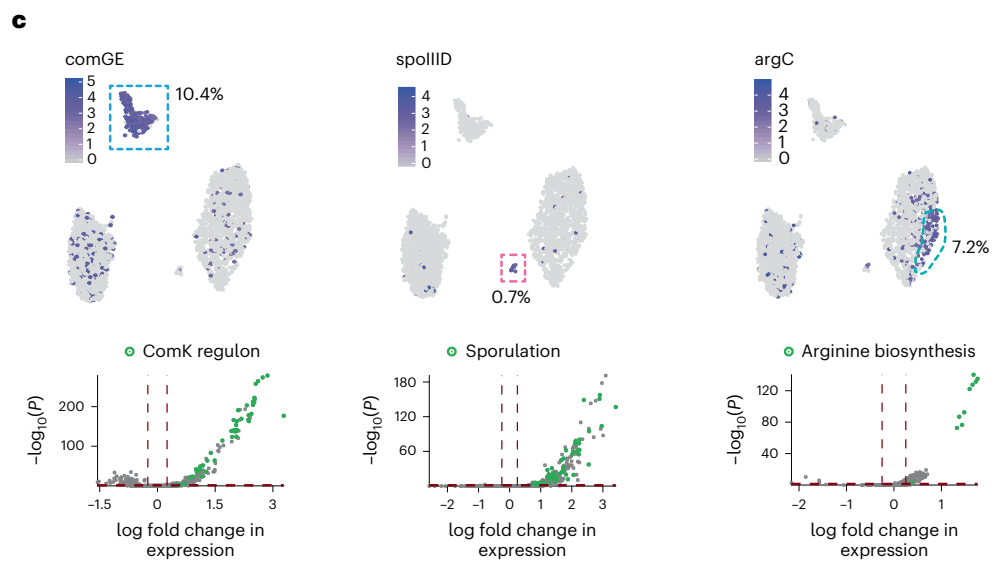
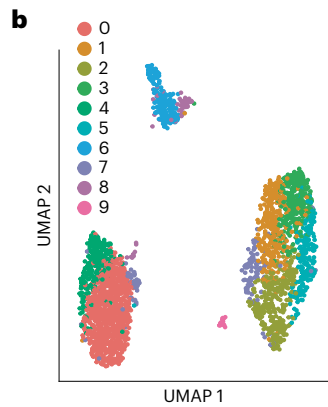
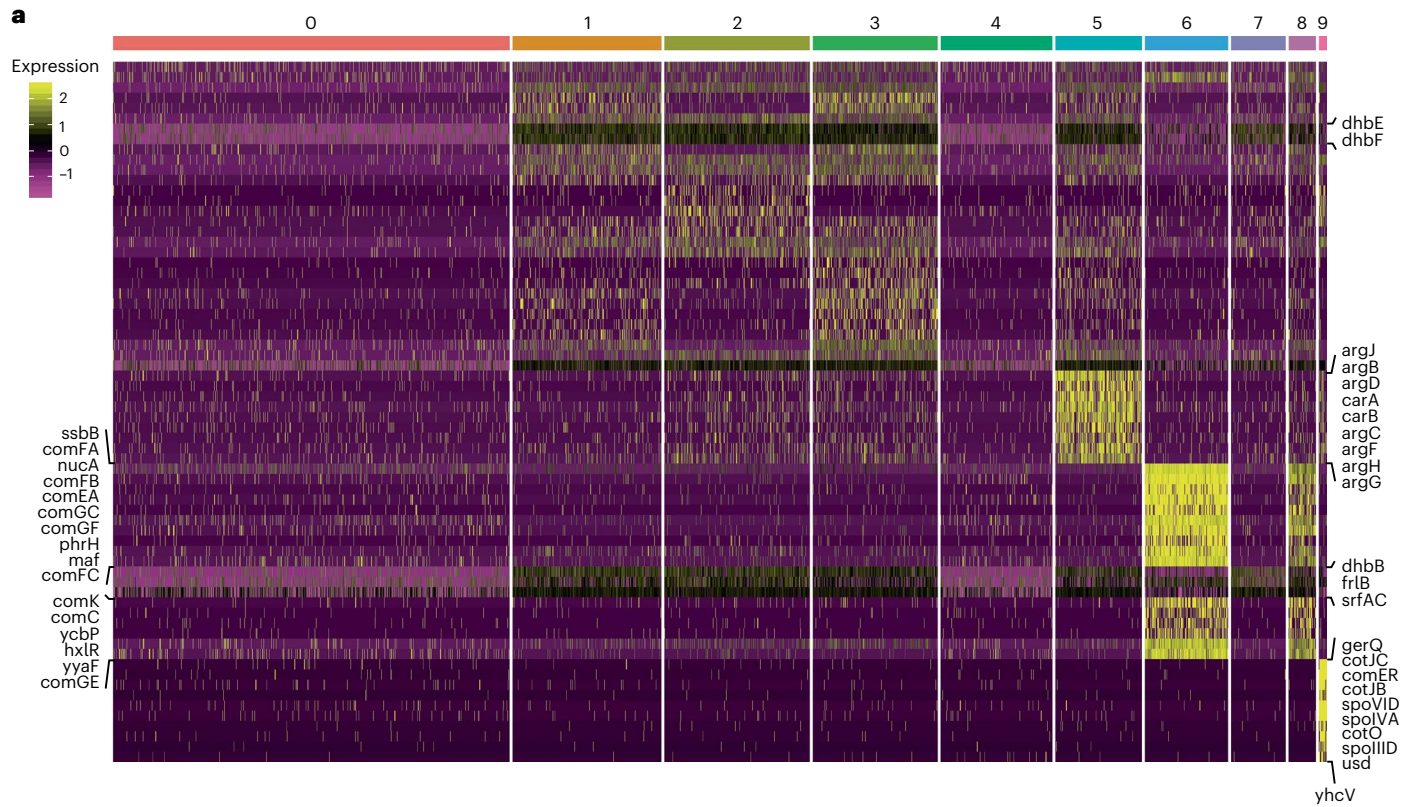
Cells within clusters 5, 6 and 7 demonstrate differential usage of carbamoyl phosphate within the culture. Clusters 5 and 7 upregulate *carA* and *carB* (\log_2 FC > 0.87, adjusted P values < 1×10^{-14}), which encode the subunits of carbamoyl phosphate synthetase, which catalyses the

Fig. 2 | ProBac-seq analysis reveals distinct transcriptional states in *B. subtilis*. **a**, Heatmap of marker gene expression (z-score of log-transformed values) from 2,784 individual *B. subtilis* cells organized into 10 clusters. **b**, UMAP two-dimensional representation of the 10 cell clusters reveals four highly distinct transcriptomic signatures. **c**, Top: single-cell expression of key marker genes for competence (*comGE*, clusters 6 and 8), sporulation (*spoIIID*, cluster 9) and arginine synthesis (*argC*, cluster 5) are highlighted on the UMAP (left to right). Cells within the highlighted cluster are boxed by dashed lines. Middle: volcano plots of genes expressed in at least 25% of cells in the corresponding clusters, with genes from the respective processes highlighted in green. P values correspond to

two-sided Wilcoxon rank-sum test with Bonferroni correction. Lower: presence of each heterogeneous marker in the population as confirmed by fluorescent promoter-reporter constructs (P_{comGE} -YFP, P_{cotY} -YFP and P_{argC} -YFP, respectively). Representative images. A phase bright spore can be seen in the *cotY*-expressing cell. Scale bars, 1 μ m. Microscope images were collected from at least ten fields with three biological replicates per reported strain to quantify phenotypes **d**, Of all *comK* regulon genes probed, 90% (45 out of 50) were significantly differentially upregulated in cell clusters 6 and 8 (Bonferroni-corrected P value ≤ 0.05 for each gene). See Supplementary Table 11 for information on *comK* regulon genes probed.

conversion of bicarbonate to carbamoyl phosphate for de novo biosynthesis of both uridine-5'-monophosphate and arginine. Both clusters, arranged adjacently on the uniform manifold approximation and projection (UMAP), also upregulate *pyrB*, *pyrC* and *pyrI*, ($\log_2FC > 0.4$, adjusted P values $< 6 \times 10^{-3}$), three enzymes involved in the first two

steps of uridine-5'-monophosphate biosynthesis, implying a commitment of the cells towards pyrimidine biosynthesis. Alternatively, cells in cluster 6 appear to shuttle carbamoyl phosphate into the arginine biosynthesis pathway as implied by the upregulation of *argB*, *argD*, *argF*, *argG*, *argI* ($\log_2FC > 0.55$, adjusted P values $< 1 \times 10^{-20}$). GSEA reinforces



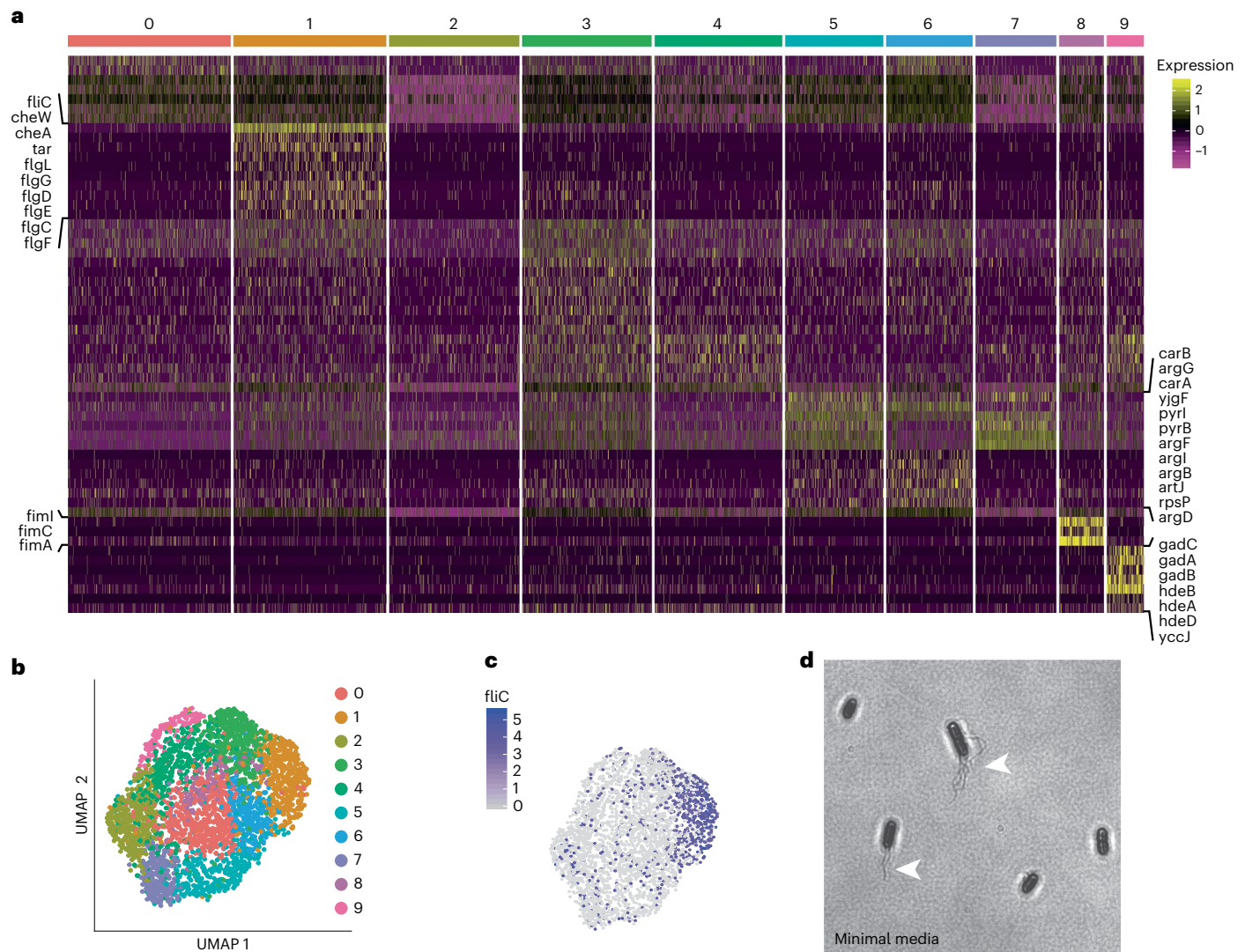


Fig. 3 | Heterogeneous gene expression in *E. coli* grown in minimal medium. **a**, Heatmap of marker gene expression (z-score of log-transformed values) from 3,315 individual *E. coli* cells grown aerobically in minimal M9 media organized into 10 clusters. **b**, UMAP two-dimensional representation of the 10

cell clusters from aerobic M9 culture conditions. **c**, Flagellar components are heterogeneously expressed in aerobic M9 media, a key flagellar gene (flagellin, *fliC*), is preferentially expressed by cells in cluster 1. **d**, The heterogeneous presence of flagella in the population is confirmed by flagellar staining.

this observation, finding a significant enrichment of genes implicated in arginine biosynthesis via ornithine in these cells (gene set fold enrichment = 26.77, FDR = 2.02×10^{-3}).

Cells in cluster 8 (141 cells, 4.3% of the population) exhibit significant upregulation of *fimI*, *fimC* and *fimA* ($\log_2FC > 2.4$, adjusted *P*value $< 1 \times 10^{-166}$). The downstream genes of the *fim* operon encode for components of type 1 pili, which are associated with biofilm formation and pathogenicity^{26–28} and are known to be expressed heterogeneously. Taken together, our observations in *E. coli* and *B. subtilis* suggest that extensive phenotypic heterogeneity is a general feature of bacteria, with processes such as arginine metabolism often confined to specialist cells. Additionally, genes associated with virulence segregate to specific cell populations, suggesting that specialized cell types may be involved in pathogenicity.

Toxin-expression heterogeneity in *C. perfringens*

After validating ProBac-seq on model organisms, we sought to examine whether we could identify distinct subpopulations in a bona fide pathogen. We focused on toxin production in *C. perfringens*, a Gram-positive,

spore-forming bacterium that is an important pathogen of humans and livestock and exhibits one of the fastest cell division times reported in literature (6.3 min)^{4,29}. The virulence factor in type A *C. perfringens* responsible for necrotic enteritis disease is a secreted β -barrel pore-forming toxin, NetB. In poultry, necrotic enteritis caused by *C. perfringens* Avian type A strain is a major challenge to antibiotic-free farming and causes annual worldwide losses of approximately US\$6 billion³⁰.

Single-cell analysis was performed on *C. perfringens* grown in rich brain heart infusion (BHI) media (Methods) to late exponential phase, when toxin is expressed. Here, we omitted inclusion of UMIs within the *C. perfringens* probe library, instead relying on the UMIs in the 10X capture oligos to quantify the number of transcripts in each cell, correcting for the overcounting induced by the in-droplet PCR (Supplementary Information and Supplementary Fig. 7). Using a custom cell-calling algorithm (Supplementary Information and Supplementary Fig. 8), 1,508 cells were resolved with an average of 507 transcripts and median of 153 transcripts detected per cell. Dimensional reduction of gene expression profiles followed by graph-based clustering

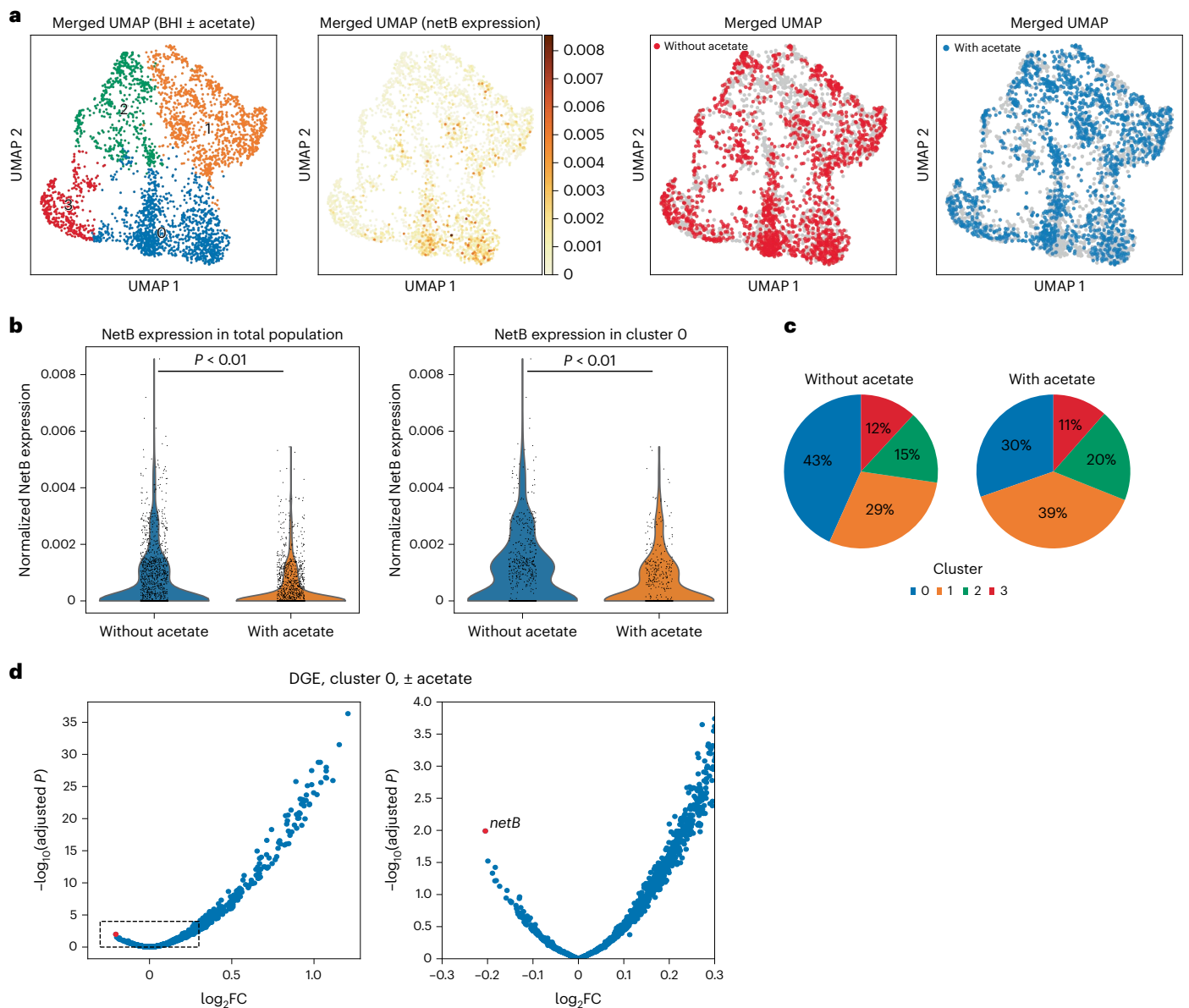


Fig. 4 | *netB* toxin in *C. perfringens* is preferentially expressed by a subpopulation of cells and can be downregulated by the addition of acetate.

a, Merged UMAP of *C. perfringens* grown in parallel to stationary phase in BHI with and without acetate (4 mM). Far left: four populations identified after graph-based clustering. Middle left: merged UMAP of *C. perfringens* with shading representing normalized *netB* toxin expression per cell. Middle right: merged UMAP in which cells grown without acetate supplementation are highlighted in red. Far right: merged UMAP in which cells grown with acetate supplementation (4 mM) are highlighted in blue. **b**, Left: violin plot of normalized *netB* expression

in all cells grown with or without acetate. P value < 0.01 by two-sided t -test. Right: violin plot of normalized *netB* expression in cells within cluster 0 grown with or without acetate. P value < 0.01 by two-sided t -test. **c**, Percentage of cells within each cluster for each condition (\pm acetate). **d**, Left: volcano plot of DGE of cells grown with versus without acetate supplementation. Counts normalized using DeSeq2 median of ratios method (ref. 45) and compared by two-sided t -test. Adjusted P values corrected by the method of Benjamini and Hochberg. Right: subset of volcano plot, focusing on genes downregulated by the addition of acetate with *netB* highlighted.

revealed four distinct *C. perfringens* subpopulations (Fig. 4a). Whereas *netB* was expressed in all clusters, differential overexpression of *netB* defined cluster 0 (Fig. 4, 43% of population, $\log_2FC = 1.12$, $P = 2.3 \times 10^{-20}$, two-sided t -test). In fact, heterogeneous *netB* expression was observed across three independent biological samples taken at different ODs around the time of transition from the exponential to stationary phase (Supplementary Table 6 and Supplementary Fig. 18).

Metabolites modulate *C. perfringens* toxin expression

For *C. perfringens* in BHI, GSEA also revealed a significant enrichment of genes involved in quorum sensing (odds ratio = 6.8, $P = 8.8 \times 10^{-5}$,

Fisher's exact test) and fatty acid degradation (odds ratio = 33, $P = 1.17 \times 10^{-5}$) in cluster 0. The agr-like quorum sensing system in *C. perfringens* is required for induction of necrotic enteritis in poultry³¹ whereas production of another exotoxin, *pfoA*, has been shown to be regulated by short-chain fatty acids such as acetate and butyrate^{32–36}.

Genes controlling fatty acid degradation were upregulated in the *netB*-overexpressing cluster whereas cluster 2 differentially expressed genes linked to fatty acid biosynthesis (odds ratio = 46.5, $P = 4.3 \times 10^{-10}$, Fisher's exact test). This led us to speculate about whether toxin production and the fraction of toxin-producing cells could be regulated by specific fatty acid metabolites such as acetate. This short-chain

fatty acid is abundant in the gastrointestinal tract and has been shown to inhibit *pfoA* exotoxin, which is controlled by a pH-dependent self-quorum quenching system^{32–36}. Thus, we hypothesized that acetate can be used to reduce *netB* expression in *C. perfringens*.

To test this hypothesis, we perturbed the *C. perfringens* extracellular environment by adding sodium acetate to the growth medium and repeated our scRNA-seq analysis at the late exponential phase. In total, 1,575 cells were captured with an average of 676 and a median of 215 transcripts detected per cell. The two datasets (\pm acetate) were merged and clustered using the same parameters as applied to the original ($-$ acetate) dataset. As before, four distinct clusters were resolved with cells from each condition dispersed throughout the clusters (Fig. 4a and Supplementary Fig. 10). Expression of *netB* was again concentrated within cluster 0 wherein cells treated with acetate expressed significantly less toxin compared to those without treatment ($\log_2FC = -0.69$, $P = 1.79 \times 10^{-9}$, two-sided *t*-test). This observation held true in the overall population as well ($\log_2FC = -0.89$, P value = 2.40×10^{-23} , two-sided *t*-test). Furthermore, the addition of acetate significantly reduced the fraction of cells in the primary toxin-producing state (cluster 0) from 43% to 30% (Fig. 4c, P value = 9.2×10^{-14} , Fisher's exact test). This reduction in toxin gene expression was consistent with a decrease in extracellular *netB* protein secreted in cultures grown in media containing acetate (Supplementary Fig. 11).

Taken together, our results with *C. perfringens* demonstrate that *netB* is differentially expressed by a specialized subpopulation of cells, and that providing growth conditions favouring alternative cell states can decrease the fraction of virulent cells in a clonal bacterial population.

Discussion

To agnostically characterize distinct transcriptional cell states within an isogenic microbial population, we developed a cost-effective bacterial scRNA-seq technique, ProBac-seq, which combines microfluidic droplet encapsulation of single cells with in situ hybridization of DNA probes for high sensitivity and throughput. Using ProBac-seq, we identified known cellular states including genetic competence and sporulation in *B. subtilis* and fimbriae production in *E. coli*. In addition, we uncovered several previously unknown transcriptional states that expressed genes that are part of metabolic pathways (amino-acid metabolism, carbon metabolism, siderophores) and physiological states (chemotaxis and motility). Strikingly, arginine biosynthesis genes appear to be preferentially expressed in distinct cell states in all three organisms that we studied.

Recently, two other methods have been proposed for scRNA-seq of bacteria: (1) sorting single bacterium into 96-well plates⁷ or (2) using a combinatorial indexing scheme on a pooled population^{5,6}. Although these techniques offer advances, they also incur scalability and capture efficiency issues. For example, low numbers of detected transcripts per cell and strand-displacement activity in random hexamer primers and reverse transcription complicate accurate quantification in combinatorial indexing methods. Additionally, both methods fail to discriminate against ribosomal RNAs, comprising more than 90% of the transcriptome. Our approach requires upfront probe generation and prior knowledge of the genome, but it is fast, cheap and provides high-resolution and accurate quantification. It uses commercial equipment that is easily available and ensures sequencing is not wasted on ribosomal or other non-mRNA transcripts (Supplementary Table 8).

Several studies have reported that toxins are expressed by a subpopulation of cells among diverse bacterial species, such as *Salmonella enterica*³⁷, *C. difficile*³⁸, *Staphylococcus aureus*³⁹ and others⁴⁰. However, these previous studies did not identify the entire transcriptomic state of toxin-producing cells. Here ProBac-seq enabled us to identify *netB* heterogeneity and gain a transcriptome-wide view of the toxin-producing and vegetative subpopulations in *C. perfringens*. We then predicted metabolites that could alter the toxin-producing cells'

physiological state, which we confirmed by measuring toxin expression and cellular states at a single-cell resolution. We anticipate that our method will be widely used to understand how external environments modulate pathogen virulence at the single-cell level in addition to bacterial transcriptional states more broadly.

Methods

Strains and growth conditions

B. subtilis str. 168 was used for all single-cell *Bacillus* experiments. M9 was supplemented with glucose and malate together as they make up the preferred carbon source for *B. subtilis*. For experiments on suspension cultures in glucose and malate, cells were grown at 37 °C with vigorous shaking in M9 media supplemented with CaCl₂ (0.1 mM), 0.2% glucose, tryptophan and trace metal mix⁸. Trace metal solution was made as a 100X concentrate using Na-EDTA 5.2 g, FeSO₄·7H₂O 2,100.0 mg, H₃BO 330.0 mg, MnCl₂·4H₂O 100.0 mg, CoCl₂·6H₂O 190.0 mg, NiCl₂·6H₂O 24.0 mg, CuCl₂·2H₂O 2.0 mg, ZnSO₄·7H₂O 144.0 mg, Na₂MoO₄·2H₂O 1,200.0 mg and DI Water, 999.0 ml. The solution pH was adjusted to 7.0. At an OD of 0.4–0.5 cultures were supplemented with 50 mM malate.

B. subtilis strain PY79 was used for all fluorescent promoter-reporter strains. *comG* reporter strain was previously described²¹. Promoter reporters for *cotY* and *argC* were made as previously described²¹. Briefly, YFP promoter reporters were cloned into the ECE174 backbone plasmid, which uses *sacA* integration site and encodes chloramphenicol resistance (R. Middleton, obtained from the Bacillus Genetic Stock Center). Strains were made by genomic integration into the genome. Fluorescent reporters were integrated into the *sacA* site and checked by sequencing. The reporter strain detail is found in Supplementary Table 5. Reporter strains were grown in the same media and growth conditions used in single-cell experiments.

E. coli MG1655 was used in all *E. coli* single-cell experiments. For experiments in minimal media cells were grown overnight in M9 minimal media and incubated at 37 °C with moderate shaking (200 r.p.m.). Overnight cultures were diluted and subcultured and a fixed specimen was collected at mid exponential phase (OD 0.3–0.5).

C. perfringens strain 25037-CP01 was grown anaerobically at 37 °C in BHI media supplemented with 0.05% cysteine-HCl and, when indicated, 4 mM of sodium acetate. Anaerobic conditions were maintained using a gas-pack and anaerobic culture boxes. The oxygen indicator on all experimental replicates indicated the absence of oxygen contamination in the chamber.

Probe set design

Probes were designed with an mRNA complementary region approximately 50 bp in length flanked by a PCR handle (18–23 bp) towards the 5' end and a 30 poly(dA) tract on the 3' end. On the ends of each probe, we included a region allowing for circularization and cutting with *hindIII* as outlined by Schmidt et al.¹². Probe sequences are included in Supplementary Tables 1, 2 and 3.

Probe amplification

Probes were amplified using a rolling circle method similar to the one used by Schmidt et al.¹² with slight modifications. To amplify our probes, we did not use nicking enzymes but instead only used the *HindIII* digestion site in the rolling circle scheme¹². Our incubations were scaled by a factor of five from the detailed protocol provided by Schmidt et al. Otherwise, all other aspects of the protocol were as previously detailed. Amplified probes were eluted and purified by PAGE electrophoresis using 15% urea gels and ethanol precipitation as described in Sambrook et al.⁴¹.

UMI and poly-A addition

Amplified 'proto-probes' were extended to include a UMI and 3' poly-adenine tail by isothermal extension with a 3' blocked primer

containing the reverse complementary sequences. In total, 100 µl of probes and 1 mg blocked extension primer (Supplementary Table 4) were mixed with 100 units of klenow fragment and 1x NEB buffer 2 and incubated for 30 min at room temperature. The extended oligonucleotide library was selectively purified by PAGE electrophoresis (final probe length approximately 142 bp) using 15% urea gels followed by ethanol precipitation as described in Sambrook et al.⁴².

Fixation and in situ hybridization reactions and optimization

Cells from 2 ml of cell culture were fixed using a 30 min incubation in 1% paraformaldehyde (final concentration) at room temperature. Formaldehyde-fixed samples were washed with 0.02% saline sodium citrate (SSC, Invitrogen) by gentle centrifugation (6,000g) for 2.5 min. After the wash, cell pellets were resuspended in 1 ml MAAM (4:1 V:V dilution of methanol to glacial acetic acid). Samples were kept at -20 °C for up to 2 days before further processing. For in situ probe hybridization, 150 µl of fixed sample was centrifuged and washed once in phosphate buffered saline (PBS) to remove methanol and acetic acid. After the wash step, cells were incubated in 200 µl PBS with 350 µl⁻¹ of lysozyme solution (Epicentre ready-lyse) for 30 min at room temperature. Lysozyme concentration was optimized and other enzyme combinations were tested to achieve a protocol with maximal probe signal and minimal cell lysis (Supplementary Fig. 12). After 30 min, cells were pelleted and washed with 500 µl PBS-tween (PBS with 0.1% Tween 20). Cells were then resuspended with 100 µl of probe binding buffer consisting of 5 × SSC, 30% formamide, 9 mM citric acid (pH 6.0), 0.1% Tween 20, 50 µg ml⁻¹ heparin and 10% low molecular weight dextran sulfate⁴². Cell suspensions were placed in a 50 °C shaker-incubator and allowed to pre-equilibrate for 1 hour. After 1 hour, 50 µl of probes (600 ng µl⁻¹) were added to each cell suspension and samples were left to incubate overnight. After the overnight incubation samples were washed five times in prewarmed (50 °C) probe-wash solution (5 × SSC, 30% formamide, 9 mM citric acid pH 6.0, 0.1% Tween 20 and 50 µg ml⁻¹ heparin). Before encapsulation on the 10X device, cells were washed three times in PBS and diluted as suggested in the 10X Chromium instruction manual. A flow cytometer was used to evaluate the retention of cells through a typical proBac-seq probe hybridization and wash procedure. Approximately 90% of fixed cells remained in solution at the end of the protocol (Supplementary Fig. 13).

Microfluidic encapsulation and droplet generation reaction

Single-cell partitioning, barcoding and cDNA library generation was achieved using the 10X Genomics Chromium Controller with the Chromium Single Cell 3' Reagents Kit (v2 chemistry) as described by 10X Genomics (<https://support.10xgenomics.com/permalink/user-guide-chromium-single-cell-3-reagent-kits-user-guide-v2-chemistry>). The protocol was modified to achieve bacterial scRNA-seq. For GEM generation (10X microfluidic encapsulation), a master mix containing the following reagents (per rxn, not accounting for excess volume) was prepared: 33 µl of 4X ddPCR Multiplex Supermix (Bio-Rad), 4 µl of custom primer (10 µM), 2.4 µl additive A (10X Genomics) and 26.8 µl dH₂O. All other reagents specified by 10X Genomics were omitted. Prepared cell samples were washed three times in PBS and diluted to 1,000 cells µl⁻¹ before loading on the microfluidic chip ('Chip A Single Cell') with a targeted cell recovery of 10,000 cells. Our recovery was lower than the expected cell number and we attribute this to the difficulty in obtaining accurate cell number measurements when working with small numbers of fixed bacterial cells.

Library construction and sequencing

After microfluidic encapsulation on the Chromium Controller, each sample (that is 'reaction') was visually inspected to confirm successful GEM formation (should observe a well distributed emulsion with a volume of approximately 100 µl). Samples were then transferred to fresh PCR tubes and cycled at the following conditions (replacing the

'GEM-RT Incubation Step' in 10X Genomics protocol): 94 °C for 5 min, six cycles of 94 °C for 30 s followed by 50 °C for 30 s then 65 °C for 30 s, held at 4 °C.

After PCR one, the emulsion was broken and the pooled DNA purified using Dynabeads MyOne Silane as described in 10X Genomics' protocol. Purified DNA was amplified once more (replacing the 'cDNA Amplification step' of 10X Genomics' protocol) using a master mix composed of 17 µl of purified DNA, 20 µl of Q5 Hot Start 2X MM, 1.5 µl of forward primer (10 µM) and 1.5 µl of reverse primer (10 µM). PCR conditions included a 30 s incubation at 98 °C followed by 16 cycles of 10 s at 98 °C, 20 s at 62 °C and 20 s at 72 °C before a final extension at 72 °C for 2 min. After PCR two, amplified DNA was purified using the NucleoSpin Gel and PCR Clean-up kit (Macherey-Nagel) as per manufacturers' instructions. Purified DNA was run on Agilent TapeStation to confirm the presence of a band at 180 bp, indicating successful library generation. Libraries were then prepared for sequencing by Illumina adaptor addition via low cycle ($n = 6$) PCR with custom library preparation finishing primers (Supplementary Table 3).

Sequencing was carried out on an Illumina nextSeq-1000 instrument with 100 cycle reagents. Libraries were spiked with 30% PhiX and sequenced for 8 bp in the i7 index direction and 119 bp for 'Read 1'. Addition of 30% PhiX improved fastQ quality scores.

RNA-seq of bulk samples

B. subtilis RNA-seq libraries used for comparison of traditional RNA-seq versus probe-based transcriptomics were first fixed with 1% paraformaldehyde for 30 min in room temperature. After fixation cells were pelleted by centrifugation (6,000g) for 5 min and formaldehyde was removed. Pellets were washed in PBS buffer. Washed cells were rehydrated in 240 µl Qiagen PKD buffer (FFPE miRNEASY kit, Qiagen). Cells were lysed by the addition of 10 µl lysosome solution for 10 min followed by bead beating using the Bullet Blender Gold and RINO beads as recommended for *B. subtilis* samples by the manufacturer. Lysed samples were further processed using the Qiagen FFPE miRNA kit. Libraries were prepared from total RNA (without removal of ncRNA) using the Takara Smart-Seq Stranded kit as per the manufacturer's instructions.

E. coli RNA-seq libraries used for comparison of traditional RNA-seq versus probe-based transcriptomics were first stabilized in Qiagen RNAprotect Bacteria reagent (or fixed in paraformaldehyde using standard single-cell protocol for half the sample that underwent probe-based analysis). RNA extraction from stabilized pellets was carried out using the standard Qiagen RNeasy kit and the recommended protocol for *E. coli* provided in the Qiagen RNAprotect Bacteria Reagent Handbook (v.HB-1704-002). Libraries were prepared from total RNA (without removal of ncRNA) using the Takara Smart-Seq Stranded kit as per the manufacturer's instructions.

Raw, demultiplexed reads were trimmed to remove adaptor regions and aligned to the relevant reference transcriptome or probe library using Bowtie2. Alignments were enumerated with featureCounts using the appropriate strandedness argument depending on the method of library preparation (Smart-seq stranded kit (Takara) or proBac-seq (this article)). Count matrices (in the form of reads per gene or probe, or reads per gene or probe per cell) were then used to quantify gene expression. For RNA libraries prepared by random priming, reads were normalized by transcript length and sequencing depth as reads per kilobase per million reads.

Microscopy

Cultures were visualized on a Leica DM3000 light microscope before single-cell experiments to ensure samples were free of chains and clumps. Reporter strains were imaged using a ×100 oil-immersion objective on a Zeiss Axio Observer inverted microscope equipped with a colibri-7 light emitting diode (LED) fluorescent light source and an axiocam digital camera. Flagellar staining was done using the

Remel flagellar stain (Thermo Fisher Scientific) as per manufacturer instructions.

Image analysis using cell segmentation and outlier identification

Cells in microscopy images were segmented using the *microbeJ* program within Fiji (ImageJ). Outliers were identified by using the IQR outlier method. Specifically, quartiles and the IQR were determined for each dataset. Outliers were determined by standard outlier detection parameters: cells that were more than 1.5 IQRs above quartile 3 were designated as cells within an overexpressing population. Population histograms were plotted and outliers reported.

Western blot analysis

To collect conditioned media from *C. perfringens* cultures at OD₆₀₀ corresponding to late exponential growth (OD₆₀₀ between 0.7 and 0.8) were pelleted by centrifugation at 4,200g for 4 min. Supernatant was then filtered through a 0.2 µm filter. Then 5 µl filtered conditioned media was incubated with NuPage LDS loading buffer (Invitrogen) for 10 min at 95 °C. Samples were loaded in equal volume and run on a 4–12% Bis Tris polyacrylamide gel. PAGE gels were transferred to an invitrolon 45 µm polyvinylidene difluoride membrane that was pre-soaked in methanol using the Xcell-II blot apparatus (Invitrogen) as per the manufacturer's instructions. Toxin netB (33 Kd) was detected using custom polyclonal rabbit antibodies (ProSci, Poway CA) at a 1:1,000 dilution and the WesternBreeze rabbit chromogenic Western Blot kit (Invitrogen). We used the SeeBlue Plus2 prestained ladder (Novex, Life Technologies) as a marker of protein size. All experiments were done using at least biological triplicates and technical triplicates on numerous independent days and representative images were selected.

Transcriptomic analysis and visualization

Single-cell gene expression matrices, *c^e*, were analysed with Seurat (v.3.1.2 with default parameters except where indicated). We first log-transformed the data using the 'NormalizeData(normalization.method = 'LogNormalize', scale.factor = 10000)' function, and selected the 2000 most variable genes using 'FindVariableFeatures(selection.method = 'vst', nfeatures = 2000)'. Then, we z-scored these highly-variable genes using 'ScaleData'. Next, we performed linear dimensionality reduction using principal component analysis (PCA) down to 50 dimensions ('RunPCA'). Points in this embedding were used to construct UMAP plots ('RunUMAP(dims = 1:10)') and find neighbours for clustering ('FindNeighbors'). 'FindClusters(resolution = 1.0)' was used to run the Louvain clustering algorithm and generate clusters. We confirmed that the clusters highlighted in the main text appeared consistently for a range of resolutions from 0.5 to 1.5. Summary statistics of the number of genes/transcripts in a cell and cluster populations for the different samples can be found in Supplementary Table 8. DGE was performed using the 'FindMarkers(min.pct = 0.25)' function with a log-fold change cutoff of 0.25, whose output when applied to our data is shown in the DGE Supplementary Tables. Heatmaps of differentially expressed genes were generated using the 'DoHeatMap' function using the standard Seurat pipeline, which displays the genes with highest scores as markers of each given cluster and show only the top overexpressed genes in each cluster with Bonferroni-corrected *P* value < 0.05. Other differentially expressed genes found in each cluster can be found in the supplementary DGE tables. For *C. perfringens* data, the above computational pipeline was repeated analogously using the Scanpy package⁴³ except for the following three steps: PCA was performed using all genes; DGE was performed with 'rank_genes_groups' function which uses two-sided *t*-test; the PAGA algorithm was run with the default parameter to obtain a graph for seeding UMAP; and we ran UMAP with the minimum distance and spread parameters set to 0.3 and 5, respectively.

Calculating corrected multiplet rate

A 'barnyard experiment' was conducted in which *E. coli* and *B. subtilis* cells were mixed at a target species ratio of 1:1 and analysed by our bacterial single-cell RNA-seq method using the 10X Chromium Controller. We recovered 3,373 GEM containing droplets with 45 (1.3%) showing evidence of interspecies collisions based on reads sharing the same cellular barcode but mapping back to different species probe sets. Assuming an exact 50:50 species mix, the true multiplet rate (accounting for both inter- and intraspecies collisions) is then estimated as $2 \times 1.3\%$, or 2.6%; that is, in experiments containing a single bacterial species, 2.6% of called 'cells' would actually represent cell multiplets. We can further correct this estimate based on the observed species ratio, following Bloom⁴⁴. In the same dataset, the number of droplets containing at least one *E. coli* cell (N1) was found to be 2,095 based on mapped reads and the number of droplets containing at least one *B. subtilis* cell (N2) was 1,323 for an observed species ratio of ~1.6:1. The number of droplets containing at least one cell of each species (N1,2) is 45, as before. Therefore, the true corrected multiplet rate can be analytically determined as 2.8%. For comparison, 10X Genomics reports an expected multiplet rate of 2.4% for 3,000 recovered cells based on the anticipated number of droplets generated per lane and Poisson loading.

Reporting summary

Further information on research design is available in the Nature Portfolio Reporting Summary linked to this article.

Data availability

All sequence data used in this publication are publicly available through the National Center for Biotechnology Information's GEO repository under accession number [GSE223752](https://www.ncbi.nlm.nih.gov/geo/query/acc.cgi?acc=GSE223752). The genome for *Clostridium perfringens* has been deposited in the National Center for Biotechnology Information under the accession numbers [CP109957](https://www.ncbi.nlm.nih.gov/nuccore/CP109957)–[CP109962](https://www.ncbi.nlm.nih.gov/nuccore/CP109962).

Code availability

Code to prepare custom references, reformat FASTQ files for the Cell Ranger pipeline, generate single-cell gene expression matrices from single-cell probe expression matrices, correct for spurious UMIs in *C. perfringens* data and perform custom cell-calling is available at https://gitlab.com/hormozlab/bacteria_scrnaseq.

References

1. Ackermann, M. A functional perspective on phenotypic heterogeneity in microorganisms. *Nat. Rev. Microbiol.* **13**, 497–508 (2015).
2. Huang, K. C. Applications of imaging for bacterial systems biology. *Curr. Opin. Microbiol.* **27**, 114–120 (2015).
3. Locke, J. C. W. & Elowitz, M. B. Using movies to analyse gene circuit dynamics in single cells. *Nat. Rev. Microbiol.* **7**, 383–392 (2009).
4. Milo, R. & Phillips, R. *Cell Biology by the Numbers* (Garland Science, 2015).
5. Kuchina, A. et al. Microbial single-cell RNA sequencing by split-pool barcoding. *Science* <https://doi.org/10.1126/science.aba5257> (2020).
6. Blattman, S. B., Jiang, W., Oikonomou, P. & Tavazoie, S. Prokaryotic single-cell RNA sequencing by in situ combinatorial indexing. *Nat. Microbiol.* **5**, 1192–1201 (2020).
7. Imdahl, F., Vafadarnejad, E., Homberger, C., Saliba, A.-E. & Vogel, J. Single-cell RNA-sequencing reports growth-condition-specific global transcriptomes of individual bacteria. *Nat. Microbiol.* **5**, 1202–1206 (2020).
8. Betin, V. et al. Hybridization-based capture of pathogen mRNA enables paired host-pathogen transcriptional analysis. *Sci. Rep.* **9**, 19244 (2019).

9. Chen, S.-H. et al. UPS 2.0: unique probe selector for probe design and oligonucleotide microarrays at the pangenomic/genomic level. *BMC Genomics* **11**, S6 (2010).
10. Gundlach, J., Rath, H., Herzberg, C., Mäder, U. & Stülke, J. Second messenger signaling in *Bacillus subtilis*: accumulation of cyclic di-AMP inhibits biofilm formation. *Front. Microbiol.* **7**, 804 (2016).
11. Wang, D. et al. The orphan gene ybjN conveys pleiotropic effects on multicellular behavior and survival of *Escherichia coli*. *PLoS ONE* **6**, e25293 (2011).
12. Schmidt, T. L. et al. Scalable amplification of strand subsets from chip-synthesized oligonucleotide libraries. *Nat. Commun.* **6**, 8634 (2015).
13. Stuart, T. et al. Comprehensive integration of single-cell data. *Cell* **177**, 1888–1902.e21 (2019).
14. Zheng, G. X. Y. et al. Massively parallel digital transcriptional profiling of single cells. *Nat. Commun.* **8**, 14049 (2017).
15. Mortazavi, A., Williams, B. A., McCue, K., Schaeffer, L. & Wold, B. Mapping and quantifying mammalian transcriptomes by RNA-Seq. *Nat. Methods* **5**, 621–628 (2008).
16. González-Ballester, D. et al. RNA-seq analysis of sulfur-deprived *Chlamydomonas* cells reveals aspects of acclimation critical for cell survival. *Plant Cell* **22**, 2058–2084 (2010).
17. Bartholomäus, A. et al. Bacteria differently regulate mRNA abundance to specifically respond to various stresses. *Phil. Trans. R. Soc. A* **374**, 20150069 (2016).
18. Ogura, M. et al. Whole-genome analysis of genes regulated by the *Bacillus subtilis* competence transcription factor ComK. *J. Bacteriol.* **184**, 2344–2351 (2002).
19. Berka, R. M. et al. Microarray analysis of the *Bacillus subtilis* K-state: genome-wide expression changes dependent on ComK. *Mol. Microbiol.* **43**, 1331–1345 (2002).
20. Dubnau, D. The regulation of genetic competence in *Bacillus subtilis*. *Mol. Microbiol.* **5**, 11–18 (1991).
21. Rosenthal, A. Z. et al. Metabolic interactions between dynamic bacterial subpopulations. *eLife* **7**, e33099 (2018).
22. Ashburner, M. et al. Gene ontology: tool for the unification of biology. The Gene Ontology Consortium. *Nat. Genet.* **25**, 25–29 (2000).
23. Carbon, S. et al. AmiGO: online access to ontology and annotation data. *Bioinformatics* **25**, 288–289 (2009).
24. Mi, H., Muruganujan, A., Ebert, D., Huang, X. & Thomas, P. D. PANTHER version 14: more genomes, a new PANTHER GO-slim and improvements in enrichment analysis tools. *Nucleic Acids Res.* **47**, D419–D426 (2019).
25. Chilcott, G. S. & Hughes, K. T. Coupling of flagellar gene expression to flagellar assembly in *Salmonella enterica* serovar typhimurium and *Escherichia coli*. *Microbiol. Mol. Biol. Rev.* **64**, 694–708 (2000).
26. Eisenstein, B. I. Phase variation of type 1 fimbriae in *Escherichia coli* is under transcriptional control. *Science* **214**, 337–339 (1981).
27. Adiciptaningrum, A. M., Blomfield, I. C. & Tans, S. J. Direct observation of type 1 fimbrial switching. *EMBO Rep.* **10**, 527–532 (2009).
28. Spaulding, C. N. et al. Functional role of the type 1 pilus rod structure in mediating host-pathogen interactions. *eLife* **7**, e31662 (2018).
29. Labbe, R. G. & Huang, T. H. Generation times and modeling of enterotoxin-positive and enterotoxin-negative strains of *Clostridium perfringens* in laboratory media and ground beef. *J. Food Prot.* **58**, 1303–1306 (1995).
30. Kiu, R. & Hall, L. J. An update on the human and animal enteric pathogen *Clostridium perfringens*. *Emerg. Microbes Infect.* **7**, 141 (2018).
31. Yu, Q. et al. The Agr-like quorum sensing system is required for pathogenesis of necrotic enteritis caused by *Clostridium perfringens* in poultry. *Infect. Immun.* **85**, e00975–16 (2017).
32. Kayama, H., Okumura, R. & Takeda, K. Interaction between the microbiota, epithelia, and immune cells in the intestine. *Annu. Rev. Immunol.* **38**, 23–48 (2020).
33. Adachi, K. et al. Metabolic dependent and independent pH-drop shuts down VirSR quorum sensing in *Clostridium perfringens*. *J. Biosci. Bioeng.* **125**, 525–531 (2018).
34. Gonçalves, P., Araújo, J. R. & Di Santo, J. P. A cross-talk between microbiota-derived short-chain fatty acids and the host mucosal immune system regulates intestinal homeostasis and inflammatory bowel disease. *Inflamm. Bowel Dis.* **24**, 558–572 (2018).
35. McCarville, J. L., Chen, G. Y., Cuevas, V. D., Troha, K. & Ayres, J. S. Microbiota metabolites in health and disease. *Annu. Rev. Immunol.* **38**, 147–170 (2020).
36. Koh, A., De Vadder, F., Kovatcheva-Datchary, P. & Bäckhed, F. From dietary fiber to host physiology: short-chain fatty acids as key bacterial metabolites. *Cell* **165**, 1332–1345 (2016).
37. Hockenberry, A. M. et al. Microbiota-derived metabolites inhibit *Salmonella* virulent subpopulation development by acting on single-cell behaviors. *Proc. Natl Acad. Sci. USA* **118**, e2103027118 (2021).
38. Garrett, E. M. et al. Phase variation of a signal transduction system controls *Clostridioides difficile* colony morphology, motility, and virulence. *PLoS Biol.* **17**, e3000379 (2019).
39. Boles, B. R. & Horswill, A. R. Agr-mediated dispersal of *Staphylococcus aureus* biofilms. *PLoS Pathog.* **4**, e1000052 (2008).
40. Davis, K. M. For the greater (bacterial) good: heterogeneous expression of energetically costly virulence factors. *Infect. Immun.* **88**, e00911–e00919 (2020).
41. Sambrook, J., Fritsch, E. F. & Maniatis, T. *Molecular Cloning: A Laboratory Manual* (Cold Spring Harbor Laboratory, 1989).
42. Choi, H. M. T. et al. Mapping a multiplexed zoo of mRNA expression. *Development* **143**, 3632–3637 (2016).
43. Wolf, F. A., Angerer, P. & Theis, F. J. SCANPY: large-scale single-cell gene expression data analysis. *Genome Biol.* **19**, 15 (2018).
44. Bloom, J. D. Estimating the frequency of multiplets in single-cell RNA sequencing from cell-mixing experiments. *PeerJ* **6**, e5578 (2018).
45. Love, M. I., Huber, W. & Anders, S. Moderated estimation of fold change and dispersion for RNA-seq data with DESeq2. *Genome Biol.* **15**, 550 (2014).

Acknowledgements

D.S. was funded in part by the Natural Sciences and Engineering Research Council of Canada (grant no. NSERC PGSD2-517131-2018). D.S. and S.H. acknowledge funding from the National Institutes of Health (NIH) National Institute of General Medical Sciences grant no. RO0GM118910, NIH National Heart, Lung, and Blood Institute grant no. R01HL158269, U19 Systems Immunology Pilot Project Grant at Harvard University and the Harvard University William F. Milton Fund. Portions of this research were conducted on the O2 High Performance Compute Cluster, supported by the Research Computing Group, at Harvard Medical School. See <http://rc.hms.harvard.edu> for more information.

Author contributions

A.Z.R. and S.H. conceived the project. R.M., S.L., M.A.B., J.P.M. and A.Z.R. performed laboratory experiments. D.S., S.H.P., R.M. and S.H. created the data analysis pipeline and supplemental analysis scripts. G.S., R.M. and J.P.M. sequenced and annotated the *C. perfringens*

genome and designed *C. perfringens* experiments. R.M., A.Z.R. and S.H. wrote the paper with input from all other authors. A.Z.R. and S.H. supervised the project.

Competing interests

A.Z.R., G.S., M.A.B. and J.P.M. are current or former employees of International Flavors and Fragrances (IFF), which filed two US patent applications (63/248657 and 63/397189) that contain data utilizing this technology to assess gene expression in microbial cells. All other authors declare no competing interests.

Additional information

Supplementary information The online version contains supplementary material available at <https://doi.org/10.1038/s41564-023-01348-4>.

Correspondence and requests for materials should be addressed to Sahand Hormoz or Adam Z. Rosenthal.

Peer review information *Nature Microbiology* thanks the anonymous reviewers for their contribution to the peer review of this work.

Reprints and permissions information is available at www.nature.com/reprints.

Publisher's note Springer Nature remains neutral with regard to jurisdictional claims in published maps and institutional affiliations.

Open Access This article is licensed under a Creative Commons Attribution 4.0 International License, which permits use, sharing, adaptation, distribution and reproduction in any medium or format, as long as you give appropriate credit to the original author(s) and the source, provide a link to the Creative Commons license, and indicate if changes were made. The images or other third party material in this article are included in the article's Creative Commons license, unless indicated otherwise in a credit line to the material. If material is not included in the article's Creative Commons license and your intended use is not permitted by statutory regulation or exceeds the permitted use, you will need to obtain permission directly from the copyright holder. To view a copy of this license, visit <http://creativecommons.org/licenses/by/4.0/>.

© The Author(s) 2023

Reporting Summary

Nature Portfolio wishes to improve the reproducibility of the work that we publish. This form provides structure for consistency and transparency in reporting. For further information on Nature Portfolio policies, see our [Editorial Policies](#) and the [Editorial Policy Checklist](#).

Statistics

For all statistical analyses, confirm that the following items are present in the figure legend, table legend, main text, or Methods section.

- | n/a | Confirmed |
|-------------------------------------|--|
| <input type="checkbox"/> | <input checked="" type="checkbox"/> The exact sample size (n) for each experimental group/condition, given as a discrete number and unit of measurement |
| <input type="checkbox"/> | <input checked="" type="checkbox"/> A statement on whether measurements were taken from distinct samples or whether the same sample was measured repeatedly |
| <input type="checkbox"/> | <input checked="" type="checkbox"/> The statistical test(s) used AND whether they are one- or two-sided
<i>Only common tests should be described solely by name; describe more complex techniques in the Methods section.</i> |
| <input type="checkbox"/> | <input checked="" type="checkbox"/> A description of all covariates tested |
| <input type="checkbox"/> | <input checked="" type="checkbox"/> A description of any assumptions or corrections, such as tests of normality and adjustment for multiple comparisons |
| <input type="checkbox"/> | <input checked="" type="checkbox"/> A full description of the statistical parameters including central tendency (e.g. means) or other basic estimates (e.g. regression coefficient) AND variation (e.g. standard deviation) or associated estimates of uncertainty (e.g. confidence intervals) |
| <input type="checkbox"/> | <input checked="" type="checkbox"/> For null hypothesis testing, the test statistic (e.g. F , t , r) with confidence intervals, effect sizes, degrees of freedom and P value noted
<i>Give P values as exact values whenever suitable.</i> |
| <input type="checkbox"/> | <input checked="" type="checkbox"/> For Bayesian analysis, information on the choice of priors and Markov chain Monte Carlo settings |
| <input checked="" type="checkbox"/> | <input type="checkbox"/> For hierarchical and complex designs, identification of the appropriate level for tests and full reporting of outcomes |
| <input type="checkbox"/> | <input checked="" type="checkbox"/> Estimates of effect sizes (e.g. Cohen's d , Pearson's r), indicating how they were calculated |

Our web collection on [statistics for biologists](#) contains articles on many of the points above.

Software and code

Policy information about [availability of computer code](#)

- | | |
|-----------------|---|
| Data collection | Sequence reads were collected on an Illumina Nextseq 2000 with default base calling software. |
| Data analysis | Custom code written in MATLAB 2019a (Mathworks) and Python (v3.8) was used to filter and reformat sequencing data and single-cell count matrices and is publicly available (https://gitlab.com/hormozlab/bacteria_scrnaseq). Cell Ranger 3.1.0 (10x Genomics) was used to obtain single-cell count matrices from sequencing data. Seurat v3.1.2 and Scanpy v1.7 packages were used to perform single-cell analyses. The DeSeq2 (v3.16) package was used for bulk differential gene expression analysis. NovoExpress v1.6.1 was used for flow cytometry analysis. Additional software packages used for manipulating/aligning sequence data include samtools v1.8, featureCounts v2.0, and bowtie2 v2.4. Figures were compiled in Adobe Illustrator 2022. |

For manuscripts utilizing custom algorithms or software that are central to the research but not yet described in published literature, software must be made available to editors and reviewers. We strongly encourage code deposition in a community repository (e.g. GitHub). See the Nature Portfolio [guidelines for submitting code & software](#) for further information.

Data

Policy information about [availability of data](#)

All manuscripts must include a [data availability statement](#). This statement should provide the following information, where applicable:

- Accession codes, unique identifiers, or web links for publicly available datasets
- A description of any restrictions on data availability
- For clinical datasets or third party data, please ensure that the statement adheres to our [policy](#)

All sequence data used in this publication is publicly available through the NCBI's GEO repository under accession # GSE223752. The genome for Clostridium perfringens has been deposited in NCBI under the accession numbers CP109957-CP109962.

Human research participants

Policy information about [studies involving human research participants and Sex and Gender in Research](#).

Reporting on sex and gender

Population characteristics

Recruitment

Ethics oversight

Note that full information on the approval of the study protocol must also be provided in the manuscript.

Field-specific reporting

Please select the one below that is the best fit for your research. If you are not sure, read the appropriate sections before making your selection.

Life sciences Behavioural & social sciences Ecological, evolutionary & environmental sciences

For a reference copy of the document with all sections, see [nature.com/documents/nr-reporting-summary-flat.pdf](https://www.nature.com/documents/nr-reporting-summary-flat.pdf)

Life sciences study design

All studies must disclose on these points even when the disclosure is negative.

Sample size

Data exclusions

Replication

Randomization

Blinding

Reporting for specific materials, systems and methods

We require information from authors about some types of materials, experimental systems and methods used in many studies. Here, indicate whether each material, system or method listed is relevant to your study. If you are not sure if a list item applies to your research, read the appropriate section before selecting a response.

Materials & experimental systems

- n/a Involved in the study
- Antibodies
- Eukaryotic cell lines
- Palaeontology and archaeology
- Animals and other organisms
- Clinical data
- Dual use research of concern

Methods

- n/a Involved in the study
- ChIP-seq
- Flow cytometry
- MRI-based neuroimaging

Antibodies

- Antibodies used
- Validation

Flow Cytometry

Plots

- Confirm that:
- The axis labels state the marker and fluorochrome used (e.g. CD4-FITC).
- The axis scales are clearly visible. Include numbers along axes only for bottom left plot of group (a 'group' is an analysis of identical markers).
- All plots are contour plots with outliers or pseudocolor plots.
- A numerical value for number of cells or percentage (with statistics) is provided.

Methodology

- Sample preparation
- Instrument
- Software
- Cell population abundance
- Gating strategy
- Tick this box to confirm that a figure exemplifying the gating strategy is provided in the Supplementary Information.